DESIGN OF THE TESTING PROCEDURE FOR INVESTIGATION OF *ERYX CONICUS* DERMAL ARMOUR CHARACTERISTICS

Blanka Žaloudková[a], Petr Koudelka[b], Petra Frýdlová[c],
Mykhailo Drozdenko[d], Jan Šleichrt[b], Daniel Kytýř[b,*]

[a] *Czech Technical University in Prague, Faculty of Transportation Sciences, Na Florenci 25, 110 00 Prague 1, Czech Republic*

[b] *Czech Academy of Sciences, Institute of Theoretical and Applied Mechanics, Prosecká 809/76, 190 00 Prague 9, Czech Republic*

[c] *Charles University, Faculty of Science, Viničná 7, 128 44 Prague 2, Czech Republic*

[d] *Czech Academy of Sciences, Nuclear Physics Institute, 250 68 Řež, Czech Republic*

[*] corresponding author: `kytyr@itam.cas.cz`

Abstract. The aim of this work is to develop an experimental method suitable for the mechanical testing of highly non-standard biological samples such as snake skin with osteoderms. The objective of the method is to determine, whether the osteoderms provide a protective function for the animal in its natural environment. For this purpose, a simulation of rodents biting the skin based on uni-axial compressive loading using a synthetic tooth as a penetrator was developed with an emphasis on integration with X-ray scanners to facilitate in-situ testing. To identify and characterise the structure of snake skin and to prove the protective function of osteoderms, all samples were subjected to high resolution X-ray computed tomography. The results of the experiments are presented in the form of stress-strain curves and a map of the tangent modulus.

Keywords: Bioinspiration, snake skin, osteoderms, mechanical testing, computed tomography, dermal armour.

1. Introduction

Biological materials and animal anatomical features in general have been an inspiration for human protection since immemorial eras. Even though the research in recent years has been more material-driven, studies show that a link can be seen between modern defensive structures and structures found in the realm of animals [1]. Thus, studying the natural animal dermal armour can be helpful in dealing with the ultimate goal of human ballistic protection, which is to find the optimum between the weight of the armour, its flexibility when worn, and, most importantly, the protection it provides against a multitude of threats. A multi-layer or multi-material body armour is one of the approaches often adopted when dealing with such a problem, but there is insufficient data available on ballistic performance [2]. Here, it is important to note that different body parts require different levels of protection, where heavy armour is needed for exposed and large profile body parts such as the head or chest, while soft armour is used in other areas to reduce the overall weight and, importantly, to allow sufficient mobility in the areas around joints (i.e., typically shoulders and hips). This is also a result of natural development that originates from anatomical solutions to survival problems in animals, where, e.g., rhinoceros species have thinner skin around their joints to achieve the best ratio of protection versus mobility [3]. Thus, by the increase of protective performance in the body armour without the inevitable weight increase with available armour types, it would be possible to provide high-end protection to more parts of the human body than front and back of the torso, which is the normal extent of protection in the commonly used armour vests or plate carriers.

In general, for a deeper understanding of all the factors and processes involved in the field of bio-inspired ballistic protection, knowledge gathering methods based on the study of nature and effective transfer of the knowledge to engineering solutions of problems involve research in numerous fields including kinematics [4], morphology [5], material science [6] and structural analysis [7]. In this work, we present an initial study paving the way for in-situ investigation of morphological and mechanical characteristics in *Eryx conicus* dermal armour as part of research aimed at verifying its existence and determining its role in protecting these snake species in their natural environment.

2. Wildlife story

In our study, we focused on rough-tailed sand boas (*Eryx conicus*). In nature, it can be found in India, Pakistan, Nepal, and Bangladesh. They are stout-bodied and medium sized reaching around 80 cm in length in adulthood, the life expectancy is 20 years or even longer. Their natural habitat includes dry and rainy areas; they shelter in deep cracks and rodent

burrows. Although they are mostly nocturnal animals, they are also found to be active during the day. They prey on rodents, lizards, ground-feeding birds, and amphibians. Their anatomically unique tail with dermal armour [8] probably plays a fundamental role in their antipredatory strategy. It is hypothesised that they use it to protect and avoid serious injuries to vital parts of their body.

We assume that two-headed snakes of the genus Eryx use their armoured tails as a deceptive target while plundering rodent nests (e. g., gerbils). Indian Gerbil (*Tatera indica*) is a rodent of the Gerbillinae subfamily that commonly shares territory with snakes. In adulthood, they can grow up to 38 cm with male species slightly larger than females. Their lifespan in captivity can reach up to 7 years; however, when living in the wild, life expectancy is just a few years as many individuals have problems surviving the first year of their life due to the hazard posed by snakes. However, nests are defended by parents with sharp edged incisors (see Figure 1) [9].

The aim of this study is to design a testing method for evaluation the protective function of osteoderms (irregular small bony elements with dimensions about $500 \times 250 \times 150\,\mu$m, see Figure 1 red) in the skin of the snake based on localised mechanical experiments coupled with detailed CT inspection to quantify relevant biomechanical parameters. As a first step, the experiment was designed to investigate the quasi-static interaction of the loading tip with real snake skin with osteoderms. The loading tip was the dimension of the gerbil incisors to make it as real as possible. Snake skin without osteoderms was used as a control.
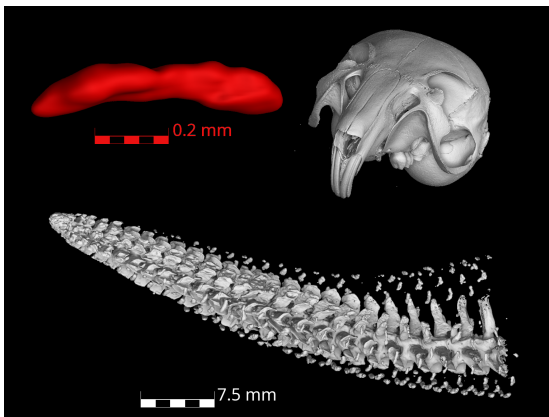

FIGURE 1. Size comparative CT based visualisation of the gerbil skull with incisors and *Eryx conicus* caudal segment with osteoderms visible as a small bony elements around the body without a tight connection to the axial skeleton together with detail of single osteoderm (in red).

3. Materials and methods

3.1. Skin samples
Four samples of the skin surface layer with thicknesses up to 500 μm of rectangular-like shape and dimensions ranging from 7×18 mm to 20×30 mm were harvested from a single individual. In the central (labelled A) and caudal (C) part of the body where the osteoderms of interest (see Figure 1) are predominantly located on the lateral (L) and ventral (V) side of the caudal segment. The samples were then long-term stored in commonly used 70 % ethanol solution [10]. The moderate effect of storage conditions on mechanical properties has been reported [11], but a more significant effect arises from the drying of the sample. For that reason, the testing procedures were performed in the shortest possible time and the samples were re-hydrated after the mechanical tests prior to X-ray imaging.

3.2. Mechanical loading
The skin samples were subjected to mechanical loading using an in-house developed compact table-top loading device presented in detail in [12] and specially instrumented for snake skin testing (see Figure 2). The upper steel loading pin with a tip cross-section of 1.25×0.4 mm was designed on the basis of the geometry assessed from an X-ray CT scan of the gerbil incisors (see Figure 1) and instrumented by LCM300 (Futek, USA) load-cell with a nominal capacity of 10 N. The lower gliding platform with the skin sample fixed by double-sided scotch tape allowed manual positioning for setting the quasi-regular the testing grid consisting of 14–20 testing points. The experiments were displacement driven up to 500 μm or interrupted when reaching the force limit of the load cell. The loading rate was set to 2 μm s^{-1}. The experiment was carried out using real-time closed loop control software [13] with 200 Hz sampling rate for both force value and encoder position readout.
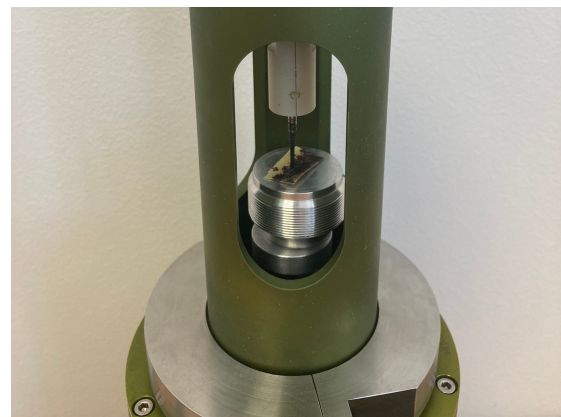

FIGURE 2. Compact table-top loading device instrumented for the snake skin testing procedure.

3.3. X-ray imaging
The modular in-house designed laboratory CT scanner, equipped with linear positioning axes and a rotary stage depicted in Figure 3, allows the exchange of the X-ray detector and source to meet specific measurement requirements. For soft, partially ossified skin

tissue, L10321 (Hamamatsu Photonics, Japan) microfocus X-ray source without additional filtering of the X-ray beam [14] together with Dexela 1512 (Varex Imaging, Germany) CMOS X-ray detector equipped with a CsI scintillator were employed. The native resolution of the detector is 1944×1536 at a pixel pitch of $74.8\,\mu$m. The imaging was performed with an acceleration voltage of $75\,$kV and a target current of $150\,\mu$A to achieve the best possible quality in the acquired radiograms. Each tomographic scan consisting of 1912 equiangular projections took approximately 30 minutes. The cone beam filtered backprojection reconstruction algorithm based on the Feldkamp-Davis-Kress method [15] implemented in VG Studio MAX 3.4.1 (Volume Graphics, Germany) was used to obtain the resulting 3D images of investigated samples having dimensions of $1536 \times 1536 \times 1944$ voxels and $20\,\mu$m effective voxel size. The histogram-based tissue segmentation procedure [16] was applied to identify the location of the osteoderm.
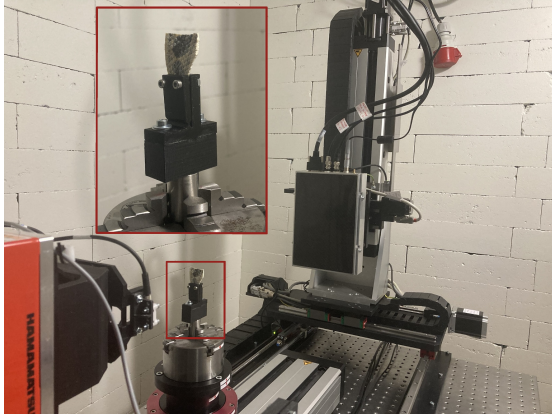

FIGURE 3. In-house designed CT setup with the X-ray source (left), detector (right) and the detail of the skin sample on rotary stage.

3.4. DATA EVALUATION

Fully automated evaluation procedure implemented in MATLAB R2023b (MathWorks, USA) was developed to calculate the stress-strain data from the measured force F and displacement u signals. For the calculation of engineering stress σ, the cross-sectional area of the nominal loading tip A_{tip} was used. The engineering strain ϵ was calculated for each measurement point individually due to the non-uniform thickness t of the sample. Here, the thickness was measured as the difference between the tip-baseplate contact t_b and the tip-skin contact position t_s, when the contact force reached $0.07\,$N at the beginning of the experiment. The stress and strain were then calculated using the equations

$$\sigma = \frac{F}{A_{tip}}, \epsilon = \frac{u}{t_b - t_s}. \tag{1}$$

To quantify the fully non-linear stress-strain behaviour of the samples, the tangent modulus was

chosen as a representative quantity. The tangent modulus was calculated using the polynomial curve fitting in the last $10\,\%$ of the strain. The results are graphically represented by stress-strain diagrams and tangent modulus values projected on the 3D image visualisation of the respective sample.

4. RESULTS

As a result of this pilot study, the results of the three samples harvested from: i) the ventral side of the central segment (AV), ii) the ventral side of the caudal segment (CV), and iii) the lateral side of the caudal segment (CL), where the osteoderms were then identified only in the CL samples. The strain stress diagrams of the AV sample are depicted in Figure 4. Invalid measurements probably caused by improper triggering of the tip-skin contact point are plotted in grey.
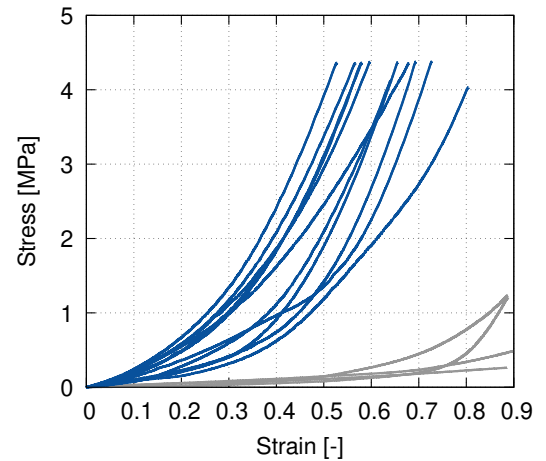

FIGURE 4. Stress-strain diagram of ventral side of central segment (AV) with 11 valid measurements presented in blue, excluded measurements in grey.

Based on 11 valid experiments, the values of the individual tangent modulus in the range of 11.48–18.66 MPa were mapped on the CT visualisation presented in Figure 5. The values are indicated by the colour and diameter of the circle with the centre corresponding to the simulated bite point. The mean value of the tangent modulus was calculated as 15.99 MPa with a standard deviation of 1.61 MPa (10.1 %).

The strain stress diagrams of the CV sample are depicted in Figure 6. Based on 13 valid experiments, the values of the individual tangent modulus in the range of 7.48–17.39 MPa were mapped on the CT visualisation presented in Figure 7. The mean value of the tangent modulus was calculated as 12.52 MPa with a standard deviation of 3.20 MPa (25.5 %).

The strain stress diagrams of the CL sample are depicted in Figure 8. Based on 3 experiments carried out on osteoderm area, individual tangent modulus values in the range of 19.15–21.70 MPa with a mean value of 20.45 MPa and a standard deviation of 1.27 MPa (6.2 %) were calculated (see Figure 9). The results of
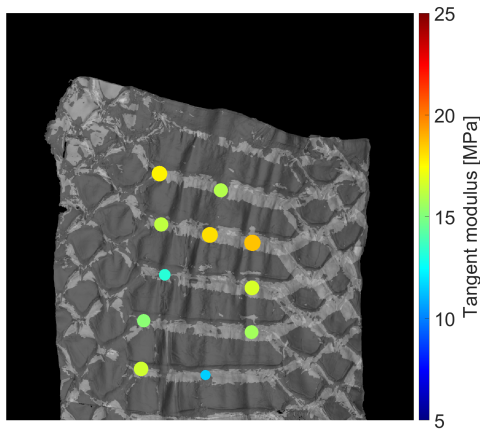
Figure 5. Localised tangent modulus magnitudes on ventral side of central segment (AV).
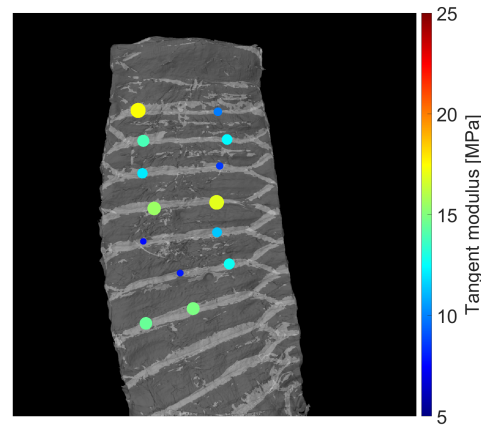

Figure 7. Localised tangent modulus magnitudes on ventral side of caudal segment (CV).
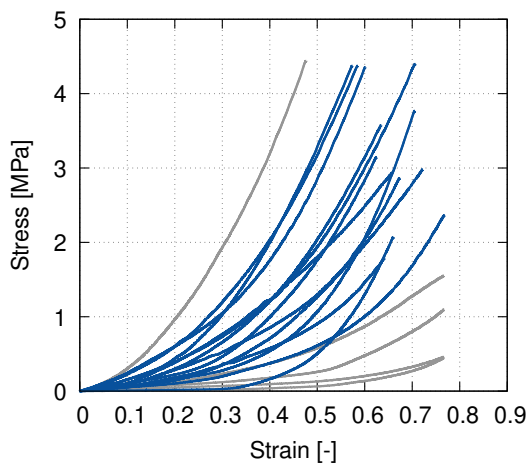

Figure 6. Stress-strain diagram of ventral side of caudal segment (CV) with 13 valid measurements presented in blue, excluded measurements in grey.
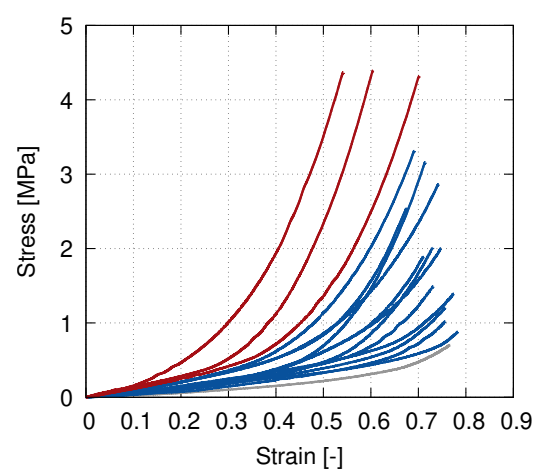

Figure 8. Stress-strain diagram of lateral side of caudal segment (CL) with 3 measurements of osteoderms and 12 measurement not influenced by osteoderms presented in blue, excluded measurements in grey.

the other 12 experiments were not influenced by osteoderms. Here, tangent modulus values in the range of 5.85–16.17 MPa with a mean value of 10.19 MPa and a standard deviation of 3.67 MPa (36.1 %) were assesed (see Figure 9).

The bite test was performed on three skin samples from a single *Eryx conicus* individual. Osteoderms were identified by CT scans only on the lateral side of the caudal segment. The average tangent modulus of the samples without osteoderms (AV, CV) was significantly higher, measuring 14.26 ± 2.45 MPa, compared to the non-ossified part of the CL, which measured 10.19 ± 3.67 MPa. For all bite tests that excluded osteoderms, the tangent modulus was calculated as 12.90 ± 2.92 MPa, while the tangent modulus in osteoderms reached 20.45 ± 1.27 MPa, although this latter value is not supported by a statistically significant number of measurements.

5. Conclusions

Based on the acquired results, it can be concluded that the proposed methodology and experimental equip-
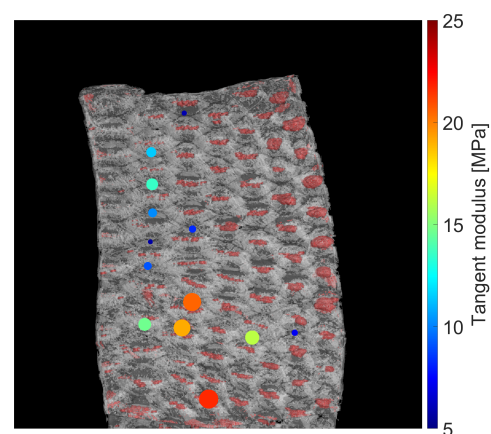

Figure 9. Localised tangent modulus magnitudes on lateral side of caudal segment (CL).

ment including the X-ray imaging chain is a viable solution to the problem of mechanical experiments and imaging of snake skin tissue equipped with dermal armour. The reconstructed 3D images from the

tomographical measurements show that it is possible to identify the osteoderms using high-resolution X-ray imaging with high confidence and to support the interpretation of the mechanical experiments. By analysing the mechanical data, the presence of osteoderms was clearly apparent, as the assessed average tangent modulus was twice as high compared to the skin without osteoderms. However, because of the geometry of the specimen and geometry of the simulated incisors, it is relatively difficult to measure the mechanical quantities precisely at the predetermined locations. The results and knowledge will be used in the following work comprising in-situ mechanical experiments during high-resolution X-ray CT imaging.

Acknowledgements

References

[1] Y. Wang, S. E. Naleway, B. Wang. Biological and bioinspired materials: Structure leading to functional and mechanical performance. *Bioactive Materials* **5**(4):745–757, 2020.
https://doi.org/10.1016/j.bioactmat.2020.06.003

[2] A. Ghazlan, T. Ngo, P. Tan, et al. Inspiration from Nature's body armours – A review of biological and bioinspired composites. *Composites Part B: Engineering* **205**:108513, 2021. https://doi.org/10.1016/j.compositesb.2020.108513

[3] Z. W. White, F. J. Vernerey. Armours for soft bodies: how far can bioinspiration take us? *Bioinspiration & Biomimetics* **13**(4):041004, 2018.
https://doi.org/10.1088/1748-3190/aababa

[4] R. Khan, M. Watanabe, A. A. Shafie. Kinematics model of snake robot considering snake scale. *American Journal of Applied Sciences* **7**(5):669–674, 2010.
https://doi.org/10.3844/ajassp.2010.669.674

[5] E. Akat Comden, M. Yenmis, D. Kytyr, et al. A study on the vertebral column of the dice snake *Natrix tessellata* (Serpentes Natricidae) from Denizli (western Anatolia, Turkey. *The Anatomical Record* **307**(5):1930–1942, 2023.
https://doi.org/10.1002/ar.25328

[6] M. Dudíková, D. Kytýř, T. Doktor, O. Jiroušek. Monitoring of material surface polishing procedure using confocal microscope. *Chemicke Listy* **105**(17):s790–s791, 2011.

[7] H. Oxlund. Relationships between the biomechanical properties, composition and molecular structure of connective tissues. *Connective Tissue Research* **15**(1–2):65–72, 1986.
https://doi.org/10.3109/03008208609001974

[8] P. Frýdlová, V. Janovská, J. Mrzílková, et al. The first description of dermal armour in snakes. *Scientific Reports* **13**(1):6405, 2023.
https://doi.org/10.1038/s41598-023-33244-6

[9] Z. Dashti, H. Alhaddad, B. H. Alhajeri. Skull variation in populations of the Indian gerbil *Tatera indica* (Gerbillinae, Rodentia) sampled across its broad geographic range. *Vertebrate Zoology* **72**:1077–1098, 2022. https://doi.org/10.3897/vz.72.e90474

[10] D. Marquina, M. Buczek, F. Ronquist, P. Łukasik. The effect of ethanol concentration on the morphological and molecular preservation of insects for biodiversity studies. *PeerJ* **9**:e10799, 2021.
https://doi.org/10.7717/peerj.10799

[11] K. S. Wu, W. W. van Osdol, R. H. Dauskardt. Mechanical properties of human stratum corneum: Effects of temperature, hydration, and chemical treatment. *Biomaterials* **27**(5):785–795, 2006. https://doi.org/10.1016/j.biomaterials.2005.06.019

[12] T. Fíla, J. Šleichrt, D. Kytýř, et al. Deformation analysis of the spongious sample in simulated physiological conditions based on in-situ compression, 4D computed tomography and fast readout detector. *Journal of Instrumentation* **13**(11):C11021–C11021, 2018.
https://doi.org/10.1088/1748-0221/13/11/c11021

[13] V. Rada, T. Fíla, P. Zlámal, et al. Multi-channel control system for in-situ laboratory loading devices. *Acta Polytechnica CTU Proceedings* **18**:15–19, 2018.
https://doi.org/10.14311/app.2018.18.0015

[14] G. E. Campillo-Rivera, C. O. Torres-Cortes, J. Vazquez-Bañuelos, et al. X-ray spectra and gamma factors from 70 to 120 kV X-ray tube voltages. *Radiation Physics and Chemistry* **184**:109437, 2021. https://doi.org/10.1016/j.radphyschem.2021.109437

[15] T. Rodet, F. Noo, M. Defrise. The cone-beam algorithm of Feldkamp, Davis, and Kress preserves oblique line integrals. *Medical Physics* **31**(7):1972–1975, 2004. https://doi.org/10.1118/1.1759828

[16] L. Lenchik, L. Heacock, A. A. Weaver, et al. Automated segmentation of tissues using CT and MRI: A systematic review. *Academic Radiology* **26**(12):1695–1706, 2019.
https://doi.org/10.1016/j.acra.2019.07.006